ISSN 1024-8560, Atmospheric and Oceanic Optics, 2017, Vol. 30, No. 3, pp. 226–233. © Pleiades Publishing, Ltd., 2017.
Original Russian Text © V.A. Korshunov, D.S. Zubachev, 2016, published in Optika Atmosfery i Okeana.

REMOTE SENSING OF ATMOSPHERE, HYDROSPHERE, AND UNDERLYING SURFACE

Characteristics of Stratospheric Aerosol from Data of Lidar Measurements over Obninsk in 2012–2015

V. A. Korshunov* and D. S. Zubachev**

Typhoon Scientific and Production Association, Obninsk, 249038 Russia

**e-mail: korshunov@rpatyphoon.ru*

***e-mail: zubachev@rpatyphoon.ru*

Received February 1, 2016

Abstract—Lidar polarization measurements of stratospheric aerosol were performed over Obninsk in 2012–2015. In all, over 300 altitude profiles of the aerosol backscattering coefficient at a wavelength of 532 nm in the altitude interval from 10 to 40 km were obtained. Overall, the measured aerosol backscattering characteristics are close to the known background values. During spring 2013, an elevated content of spherical-type aerosol was noted in the tropopause region, seemingly associated with sedimentation of aerosol structures formed during the fall of the Chelyabinsk meteorite. In July 2014 and 2015, layers of increased aerosol scattering were observed in the altitude interval from 10 to 15 km, associated with transcontinental transport of aerosol from Canadian forest fires. Integrated backscattering and extinction characteristics are estimated for the lower (from tropopause level to 15 km) and middle (from 15 to 30 km) stratospheric layers. It is found that the contribution of the lower layer to these optical characteristics is 1.8 and 1.6 times larger than the contribution of the middle layer.

Keywords: stratosphere, lidar, aerosol, backscattering, optical depth, Chelyabinsk meteorite

DOI: 10.1134/S1024856017030083

INTRODUCTION

The monitoring of stratospheric aerosol plays an important role in atmospheric studies because aerosols affect the radiation processes and, possibly, the climate of the Earth. The lidar method is one of most efficient tools for solving this problem. Over a long time, regular measurements were performed at the Siberian Lidar Station in Tomsk [1], in Garmisch-Partenkirchen (Germany) [2], and other research centers. Stratospheric aerosol sensing was carried out in the Typhoon Scientific and Production Association, Obninsk, for 12 years from 1984 to 1996 [3]. At present, measurements at the Obninsk lidar station have been resumed on a new basis with the help of AK-3 lidar, developed at Typhoon and permitting complex measurements of aerosol, ozone, and temperature of the middle atmosphere. In the present paper, we describe the results of aerosol measurements performed in 2012–2015. Changes in the state of stratospheric aerosol that took place at that time are discussed, and examples of transcontinental aerosol transport in the stratosphere are presented.

INSTRUMENTATION AND METHOD OF MEASUREMENTS

The stratospheric aerosol sensing was performed in the altitude range from 10 to 40 km. A Nd:YAG laser was used as a transmitter; and since 2014, two such lasers have been operating simultaneously, with maximal energies of 180 and 480 mJ per pulse at wavelengths 355 and 532 nm. The diameter of the receiver mirror was 635 mm. A four-channel receiving system, comprising four channels with different transmissions at wavelength 355 nm and two polarization channels at wavelength 532 nm with parallel and perpendicular polarizations of sensing radiation, operated in the photon counting mode. Measurements were performed at nighttime. A mechanical cutoff of near-field zone was used.

To cover the entire range of distances from 10 to 40 km, the aerosol measurements were performed in two stages, each 30 min long, and each with a different setting of cutoff distance of the near-field zone (below 10 and below 16 km) and different energies of the transmitter. This sensing method was chosen because layers with elevated scattering are often observed near the tropopause, thereby increasing the dynamic range of signals recorded. At the same time, there is only a single recording channel for each polarization at a wavelength of 532 nm. Signals in two measurements for each wavelength and polarization were sewn during signal processing. As a result of processing, we determined the altitude profiles of aerosol backscattering coefficient $\beta_a(h)$ and backscattering ratio $R(h) = [\beta_a(h) + \beta_R(h)]/\beta_R(h)$, where $\beta_R(h)$ is the Rayleigh backscattering coefficient.

Just after aerosol measurements, we performed two-wavelength sensing by the method of modified Rayleigh scattering in the altitude range from 30 to 70 km, the result being the altitude profiles of temperature and backscattering ratio [4]. The backscattering ratios obtained were used for referencing signals from aerosol measurements in the altitude range from 35 to 40 km. The method of aerosol signal processing was based on known Fernald–Klett solutions, with altitude profile of lidar ratios specified based on an optical-microphysical model of stratospheric aerosol [5]. The measurement errors were estimated by the Monte Carlo method, taking into account the statistical fluctuations during signal photo recording, as well as the a priori uncertainty of signal referencing at a reference point of the sensing path. We will further consider only results of measurements at 532 nm because, as will be clear below, most measurements pertain to background conditions, and aerosol backscattering coefficients are small compared to the Rayleigh backscattering coefficients at the wavelength of 355 nm.

Ozone absorption should be taken into consideration in signal processing at 532 nm [2], especially for conditions close to background. Our estimates show that the neglect of ozone absorption leads to a bias in the backscattering ratio, which increases from the reference point (generally chosen at the end of the sensing path) down the sensing path. This bias reaches a value on the order of +0.038 at a height of 12 km, given the characteristic integrated ozone content of 250 DU on the sensing path. The corresponding biases of the integrated backscattering coefficient are 5×10^{-5} sr^{-1} in the interval 15–30 km.

Ozone absorption cross section at a wavelength of 532 nm was specified on the basis of measurements [6–8] and data presented in the MPI-Mainz-UV-VIS Spectral Atlas database [9]. A cross section of $(2.85 \pm 0.01) \times 10^{-21}$ cm^2 is assumed for the temperature range (220 ± 10) K. We note that the absorption cross section is more than an order of magnitude larger at 532 nm than at 355 nm.

ALTITUDE PROFILES OF AEROSOL BACKSCATTERING COEFFICIENTS

Stratospheric aerosol measurements using the AK-3 lidar were first performed in August 2011. In all, over 300 measurements were carried out until mid-2015. Figure 1 shows the average altitude profiles of $\beta_a(h)$ at a wavelength of 532 nm in the altitude range from 12 to 40 km for winter (December–February) seasons of 2012–2013, 2013–2014, and 2014–2015, and for summer (May–August) seasons of 2013, 2014, and 2015.

The errors of $\beta_a(h)$ were estimated through errors of $R(h)$. When $R(h)$ is close to unity, we have $\delta[\log\beta_a(h)] = 0.43\delta R(h)/(R(h)-1)$ [5]. Numerical estimates of $\delta R(h)$, obtained using a Monte Carlo method for real experimental profiles, show that $\delta R(h)$ weakly depends on the height for a single measurement and can be assumed to be equal to 0.02. When the average is taken over many profiles, the uncertainty of the average decreases. Figure 1 shows the error corridor $\delta[\log\beta_a(h)]$ for the average profiles of $\beta_a(h)$ under the assumption of the random character of errors of single measurements (solid curve, surrounded from two sides by dashed curves). Error bars indicate errors of a single measurement. Actual error of the average profiles lies somewhere in between the two estimates.

For comparison purposes, Fig. 1 shows a background altitude profile (no. 1) calculated from data of in situ measurements which were used to construct the optical-microphysical model of the stratospheric aerosol [5]. In calculating this profile, from the entire dataset we selected only those measurements for which the integrated aerosol backscattering coefficient $B_\pi(532)$ in the layer from 15 to 30 km did not exceed 2×10^{-4} sr^{-1}. In addition, Fig. 1 presents the exponential model of background altitude profile (no. 2), developed at the Siberian Lidar Station according to the data of measurements in 1989–1990 [10].

In the measured profiles (Fig. 1), we can discern the characteristic minimum at heights of 28–30 km and the poorly defined Junge layer in the altitude range from 20 to 25 km. From Fig. 1 it can be seen that, on the whole, the measured profiles lie on background model no. 1 within the measurement accuracy. Marked deviations toward larger values are noted in the lower stratosphere during 2013, as well as during summer periods of 2014 and 2015 in the middle stratosphere at heights from 24 to 30 km. With respect to model no. 2, all profiles deviate toward smaller values, to some degree.

The altitude behavior of backscattering characteristics below 12 km should be plotted with respect to the tropopause layer, with aerosol layers, characterized by a high depolarization degree of aerosol backscattering, being classified into a separate group. These layers often have a backscattering maximum below the tropopause height and, as such, can be considered as cirrus cloud tops. The average height of the point of temperature minimum (henceforth, tropopause level) was about 11 km in our measurements. Figure 2 presents the averaged altitude profiles of the quantity $R - 1 = \beta_a/\beta_R$ versus the height above the tropopause level h_t. The averaging periods are chosen in accordance with date of Chelyabinsk meteorite fall on February 15, 2013, because in our measurements we recorded an elevated backscattering level in the tropopause region during spring 2013, and sometimes even in early summer 2013. In this regard, we chose the follows averaging periods: period before the meteorite event from December 1, 2012, to February 14, 2013, (Fig. 2a), period after meteorite event from February 15, 2013, to April 30, 2013, (Fig. 2b), and a subsequent period free of the meteorite effect from early 2014 to mid-2015 (Fig. 2c).

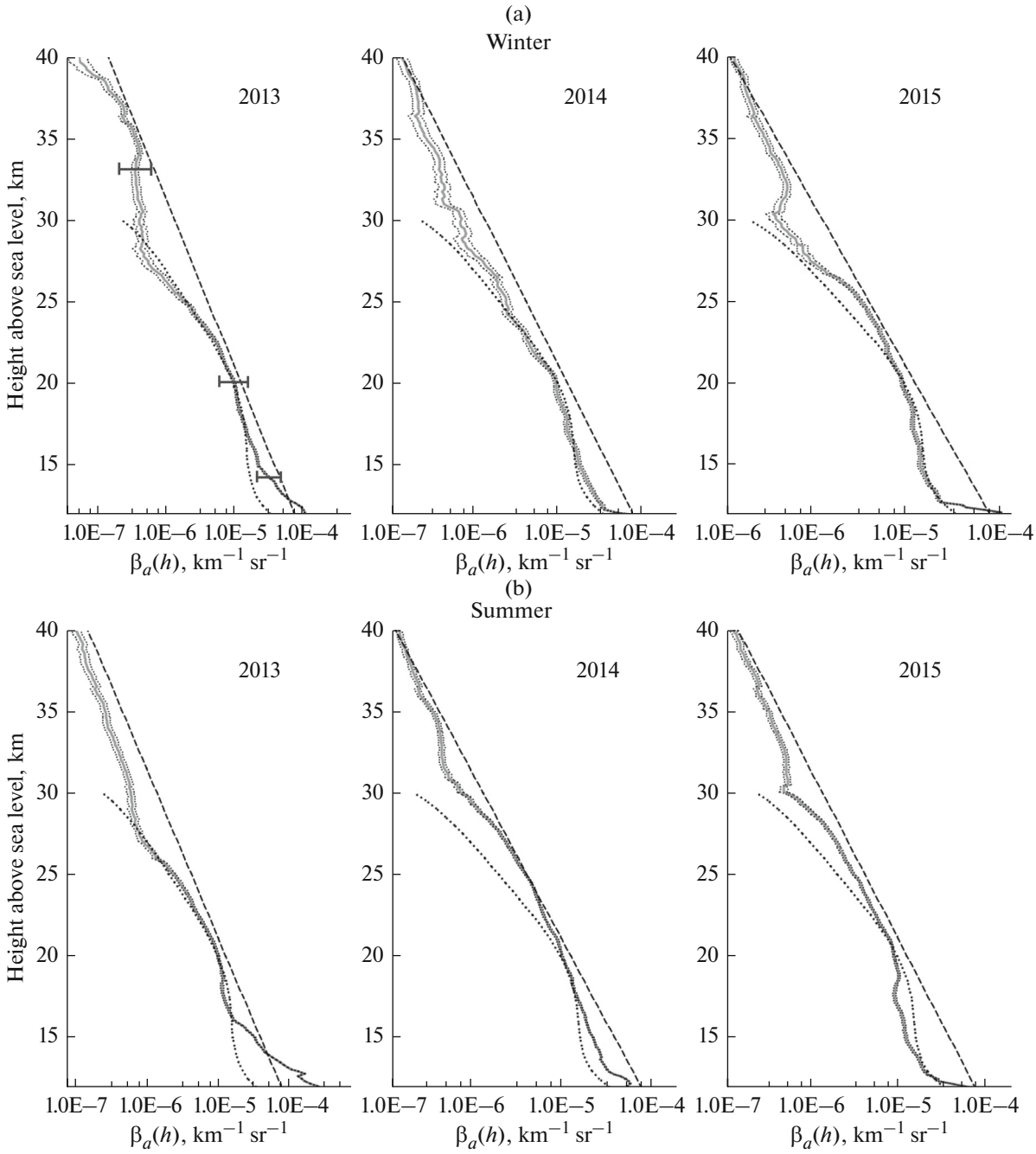

Fig. 1. Seasonal average profiles of aerosol backscattering coefficient (solid lines with error corridor of the average) for (a) three winter (2012–2013, 2013–2014, and 2014–2015) and (b) three summer (2013, 2014, 2015) seasons as compared to model-based altitude profiles. Dotted lines show background profile in the optical-microphysical model [5] (profile no. 1), and dashed lines show exponential model [10] (profile no. 2). Error bars indicate the errors of a single profile.

All profiles are divided into two classes according to the depolarization degree of aerosol backscattering $d_a(h_t)$ at the point of the maximum of backscattering ratio $h_{\max}$. The profiles with $d_a(h_{\max}) < 0.2$ are classified into a type of preferential spherical aerosol and shown by solid lines in Fig. 2; while those with $d_a(h_{\max}) > 0.2$ are classified into a crystalline type and shown by dashed lines. From Fig. 2a and c both before the meteorite event, and in period of 2014–2015, $R(h_t) - 1$ was much less for the spherical than for crystalline aerosol, and was at the level of ~0.1. Comparison with altitude profile of $R(h) - 1$ in a wider altitude range shows that, for the spherical aerosol, the value of $R(h) - 1$ at the tropopause level is, on average, comparable to that in the Junge layer. The situation had

changed in 2013 after the meteorite fall (Fig. 2b); in that period, the $R(h_t) - 1$ value increased for a spherical-type aerosol by an order of magnitude; at the same time, for crystalline structures, the $R(h_t) - 1$ value even decreased.

Measurements indicated [11] that, according to the depolarization degree of backscattering, the meteor aerosol was close to the spherical type ($d_a < 0.1$). Therefore, the formation of a spherical-type layer with elevated scattering in the tropopause region can be interpreted either as a direct result of meteor aerosol sedimentation or as a sulfur acid aerosol layer thickening on meteor condensation nuclei.

AEROSOL STRUCTURES IN THE REGION OF TROPOPAUSE INVERSION LAYER

The analysis of altitude profiles of temperature, obtained from radio sensing data on days of lidar measurements, shows that the inversion layer, known in the literature as the tropopause inversion layer (TIL), is often observed in the tropopause region. The TIL region above the tropopause occupies about 2 km, with the inversion, on average, being 4° in magnitude. Data in works [12, 13] indicate that the TIL phenomenon occurs rather frequently and is globally widespread. The origins of this layer are now under active debate.

The presence of TIL may favor the aerosol accumulation immediately above the tropopause. In our measurements, this is supported by the fact that the maximum of aerosol scattering is often observed not at a temperature minimum, but, rather, in regions above, i.e., in the TIL region. According to our measurements, we determined the probabilities of observation of elevated scattering layers (with the maximal value $R(h_t) - 1 > 0.2$) in the tropopause region. Measurements from February 15, 2013, to January 1, 2014, as potentially subject to the meteor aerosol effect, were excluded from all measurements performed. In all, 242 measurements remained for analysis. It turned out that crystalline-type elevated-scattering layers were observed above the tropopause in 20% of cases, and spherical-type layers were observed in 13% of cases. The TIL phenomenon was observed in 56% of the total number of measurements. We verified is there a relationship between spherical-type aerosol and TIL presence. The probability of observation of aerosol in the presence of TIL was estimated using Bayes theorem: $P(A/B) = P(AB)/P(B)$, where A is the event of observation of an aerosol layer ($R > 1.2$; $d_a < 0.2$) in the tropopause region, and B is the event of TIL observation. It was found that $P(A/B)$ is 18%, while the unconditional probability of aerosol observation $P(A) = 13\%$. Thus, the probability of observation of the elevated-scattering layer increases by 39% in the presence of TIL; therefore, data indicate that there is a positive correlation between aerosol structures and TIL.

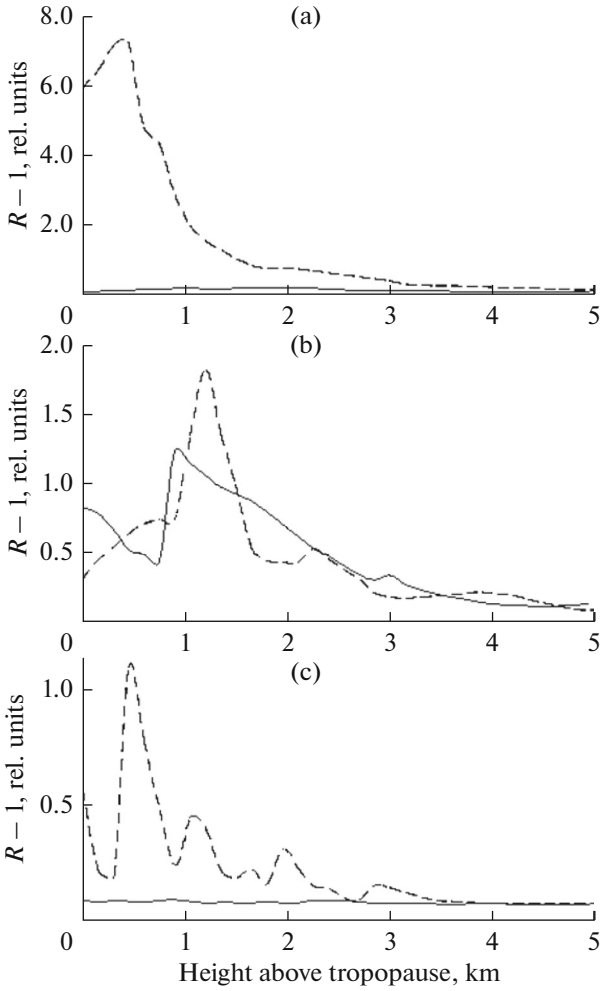

Fig. 2. Altitude profiles of backscattering ratio $R(h_t)$ for spherical (solid lines) and crystalline (dashed lines) aerosols.

INTEGRATED OPTICAL CHARACTERISTICS OF STRATOSPHERIC AEROSOL

The degree of stratospheric aerosol loading is generally estimated according to the integrated aerosol backscattering coefficient $B_\pi(532)$ in the layer from 15 to 30 km. The time behavior of $B_\pi(532)$, obtained in measurements, is shown in Fig. 3. Each symbol represents a separate measurement. The gap in the measurement record in 2013 was due to lidar modernization. The solid curve shows sliding averaging over measurements, performed within ±15 days of the current date. The average $B_\pi(532)$ values were 0.94×10^{-4} sr^{-1} (in the first half of 2013); 1.07×10^{-4} sr^{-1} (2014); and 0.98×10^{-4} sr^{-1} (in the first half of 2015). The $B_\pi(532)$ value, averaged over all measurements, was 1.06×10^{-4} sr^{-1}, with a standard deviation of 0.39×10^{-4} sr^{-1}. Table 1 presents the literature data on $B_\pi(532)$ value [10^{-4} sr^{-1}], which are considered as background values. Data for Tomsk (1997–2006) are those from work [1]; and the

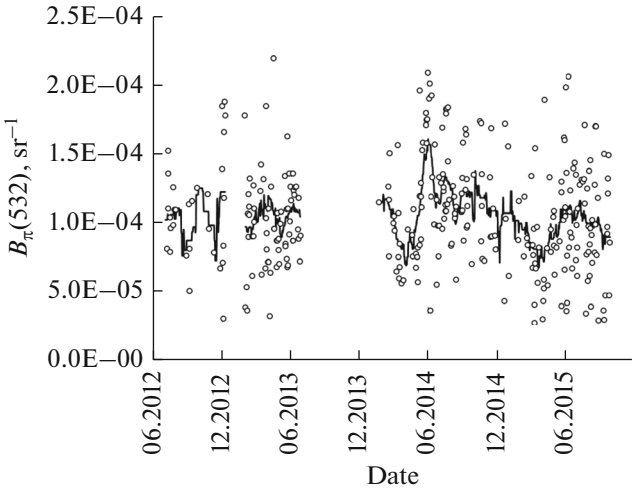

Fig. 3. Time behavior of integrated aerosol backscattering coefficient $B_\pi(532)$.

other data are from work [14]. Comparison of our measurements with those presented in Table 1 shows that, in the period of 2013–2015, the aerosol content in the region of the main aerosol layer of 15–30 km can be considered to be close to background level.

We will consider how the results compare with the known data on volcanic eruptions. As is well known [1, 2], the quiescent (background) state of the stratospheric aerosol was observed from 1999 to 2005. After 2005, several moderately strong eruptions produced an increase in aerosol content in the stratosphere [1, 15]. The volcanic activity has again declined since 2012: the yearly volcanic SO_2 emission in 2012–2015 did not exceed 0.6 Mt, according to data of work [16]. It is noteworthy that most considerable eruptions occurred in the Southern hemisphere (Kelud volcano, 8° S, 112° E, February 13, 2014, 136 kt of SO_2 injected). Volcanoes of Pacific Ring of Fire (Shiveluch, Zhupanovsky, etc.) had episodically erupted, ejecting products to the height of 10 km and higher. The total numbers of such eruptions, which we estimated according to data of work [17], had been 4, 12, and 9 in 2013, 2014, and 2015, respectively. Considering that a westerly wind dominates in the lower stratosphere, these eruptions seem to have exerted no immediate effect on the aerosol content of the main stratospheric layer over Obninsk. For this same reason, the aerosol transport could not be traced with the help of back trajectory analysis.

Table 1. Background levels of integrated backscattering coefficient $B_\pi(532)$ [10^{-4} sr^{-1}] according to measurements at five lidar stations

Tomsk	Sao Jose	Mauna Loa	Yampton	Garmish
1.5	0.83	0.68	0.85	0.55

Table 2. Integrated optical characteristics of the middle (15–30 km) and lower (h_{tr} – 15 km) aerosol layers of the stratosphere

Parameter	Lower layer	Middle layer
τ	7.51E-03	4.81E-03
τ_{sph}	6.79E-03	
τ_{cr}	1.09E-02	
B_π	1.93E-04	1.07E-04
$B_{\pi\,sph}$	1.50E-04	
$B_{\pi\,cr}$	3.85E-04	

The average time dependence of $B_\pi(532)$ (see Fig. 3) exhibits no typical seasonal behavior with the wintertime maximum of aerosol content. We note that the absence of seasonal differences is considered as a signature of the background state of the aerosol layer [10]. Instead, we see springtime minima, as well as the summer maximum in 2014. Our estimates confirmed the nonrandom character of these bursts at less than 0.001 significance level. The summer maximum in 2014 seems to be due to activation of forest fires in Canada and the United States, when pyrocumulus clouds formed with aerosol ascent to the stratosphere and with possible far-range aerosol transport [18, 19].

In the recent work [20] it was pointed out that the region of the lower stratosphere from tropopause to 15 km may have a significant contribution to the optical depth of the stratospheric aerosol layer, which should be taken into consideration in climate models. In this regard, the results of our measurements were used to compare the optical parameters at a wavelength of 532 nm for two layers: from the tropopause to 15 km, and from 15 to 30 km. The averages over all our measurements (except in time of the possible effect of meteorite aerosol) are presented in Table 2, where τ is the optical depth of these layers. The τ values were determined separately for classes of crystalline and spherical aerosol structures and indicated by subscripts "cr" and "sph". Analogous notations are used for integrated backscattering coefficients B_π. The τ estimates were obtained using the extinction coefficient $\sigma(h, 532)$ determined from the formula $\sigma(h, 532) = \chi\beta_a(h, 532)$, where χ is the lidar ratio. Depending on polarization of radiation and particle orientation, χ in crystalline clouds can vary in quite wide limits (20 ± 10); however, it is close to 20 in most cases, based both on field observations [21–23] and on results of measurements in an aerosol chamber [24]. For spherical sulfuric acid aerosol, our calculations for background conditions based on model [5], as well as data presented in [25], give identical results: χ varies with altitude in the range (45 ± 5). Accordingly, in $\sigma(h, 532)$ estimation, χ was assumed to be 20 at those points h, where $d_a(h) > 0.2$; it was assumed to be 45 for the points h where $d_a(h) < 0.2$.

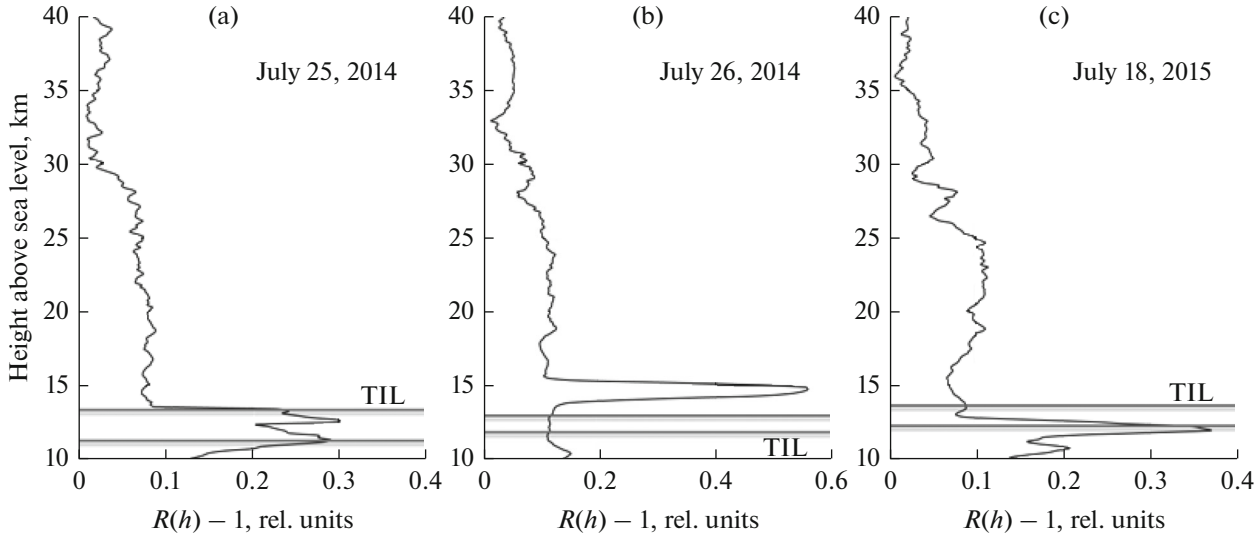

Fig. 4. Vertical profiles of backscattering ratio $R(532)$, obtained on July 25 and 26, 2014, and July 18, 2015; the horizontal lines indicate the position of the TIL layer.

From Table 2 it follows that, under background conditions, the contribution of the stratospheric layer between the tropopause and 15 km to the integrated optical characteristics of backscattering (extinction) is a factor of 1.8 (1.6) larger than the contribution of the middle stratospheric layer from 15 to 30 km. The total optical depth of stratospheric aerosol, measured from h_{tr} to 30 km, is estimated at 0.012 for background conditions, with the relative contribution of the lower layer being about 60%.

Backscattering of crystalline aerosol structures at the layer maximum exceeds that of spherical aerosol structures by an order of magnitude or more (Fig. 2); however, as can be seen from Table 2, in terms of the integrated B_π, the crystalline structures exceed the spherical ones by only a factor of 2.6. When we pass to the optical depth, this relationship decreases to 1.6 because of the difference in lidar ratio between the crystalline and spherical parts of the profiles.

These estimates of the optical depths of stratospheric aerosol, as well as the relative contribution of the lower stratospheric layer (h_{tr}, 15 km), satisfactorily agree with lidar measurements in Tomsk and Tsukuba (Japan) [20].

OBSERVATIONS OF TRANSCONTINENTAL TRANSPORT OF AEROSOL FROM FOREST FIRES

Back trajectory analysis sometimes makes it possible to trace the origins of the layers of elevated aerosol scattering in the tropopause region, such as was the case in episodes of observations on July 25 and 26, 2014, as well as on July 18, 2015. Figure 4 shows the altitude distribution of $R(h) - 1$ in aerosol layers with elevated scattering. The horizontal lines indicate the TIL position. As can be seen from Fig. 4, layers are located either immediately in the TIL region or above it. The maximal depolarization degree was 0.1 in the layers in 2014 and 0.07 in the layer in 2015, indicating that these aerosol layers mainly contained spherical-type aerosol for quite high backscattering values.

Back trajectories were constructed using the HYSPLIT program available at the NOAA website [26]. We used the ensemble method of trajectory calculation in which a set of trajectories is constructed by varying the initial grid point. The obtained ensembles of back trajectories for July 25, 2014, and July 18, 2015, are shown in Fig. 5. The trajectories were constructed with a time interval of 10 days in the backward direction from observation time in Obninsk (about 20:00 UTC). The end of trajectories for July 25 corresponded to those of July 15 (20:00 UTC), or, taking into account the time shift (~7 h), to approximately local noon of July 15. It is just on those days, i.e., on July 14–15, severe forest fires were observed in the northwestern provinces of Canada. Traces of pyrocumulus formation were distinctly seen in satellite images [27]. The fire area in Fig. 5 is indicated by a rhombus.

From Fig. 5, it can be seen that a major group of trajectories reaches the forest fire zone by July 15. Therefore, it is highly probable that these layers are associated with the outflow of fire products to the stratosphere in the process of pyrocumulus formation. For the date of measurements on July 18, 2015, the backward trajectories partially end in the region of Hudson Bay (rhombus in Fig. 5b), along the coasts of which severe forest fires were also observed on July 7–8 [28]. These cases, when aerosol layers with elevated scattering were observed, with a high probability can be associated with a transcontinental transport of smoke aerosol from forest fires in the stratosphere.

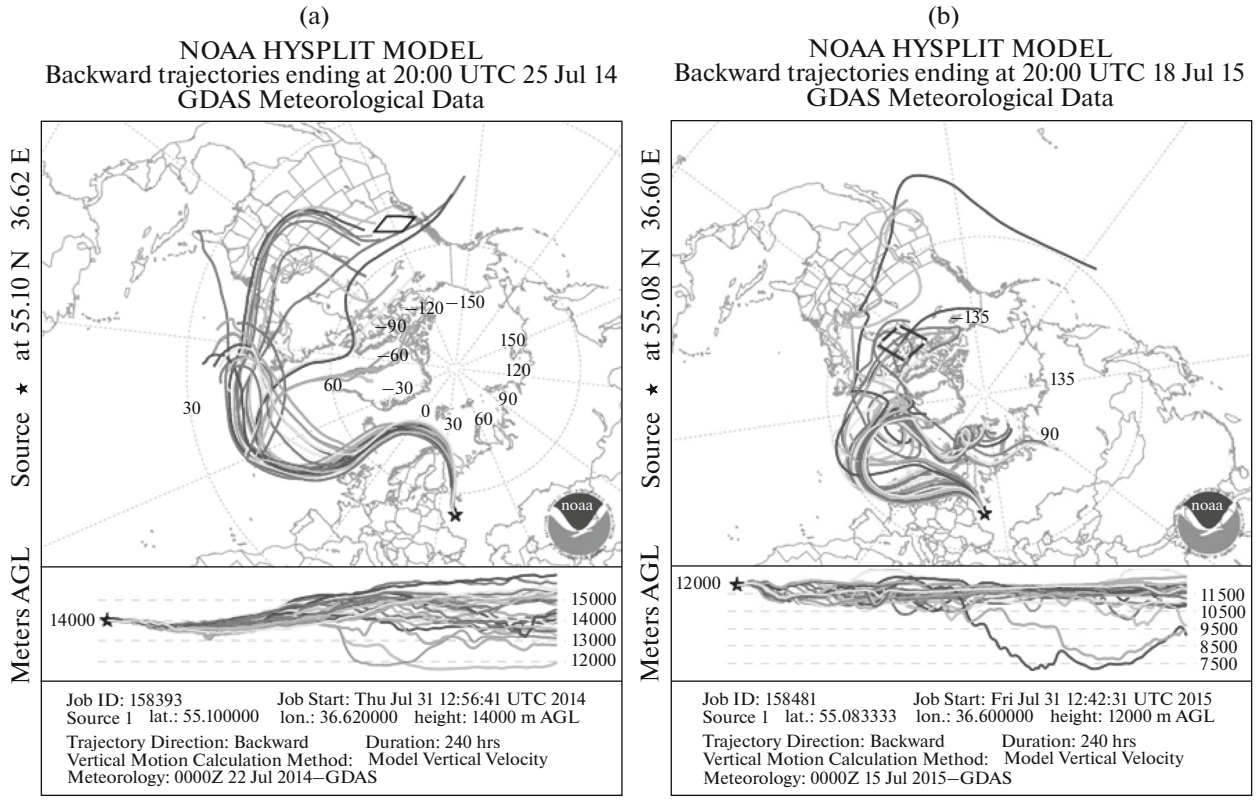

Fig. 5. Backward trajectory ensembles for 10 days backward from the date of measurements on (a) July 25, 2014, and (b) July 18, 2015. Rhombuses indicate the zones of severe forest fires with pyrocumulus formation.

CONCLUSIONS

Lidar measurements of stratospheric aerosol over Obninsk were performed in 2012–2015. In all, more than 300 altitude profiles of the aerosol backscattering coefficient at a wavelength of 532 nm were obtained. Seasonal average profiles in the layer from 15 to 30 km are mostly close to the background profiles, calculated according the known data of in situ microphysical measurements in the framework of the previously developed model of stratospheric aerosol [5]. The average values of the integrated aerosol backscattering coefficient in the layer of 15–30 km agree well with data of known lidar measurements for earlier observed background periods. The results obtained correspond well to the available evidence of the reduced volcanic activity in the period considered here.

Deviations from background profiles were noted during the spring and summer of 2013 in the tropopause region, as well during the summers of 2014 and 2015 at heights above 25 km. The elevated content of spherical-type aerosols, observed over the tropopause during spring 2013, seems to be associated with sedimentation of aerosol structures that appeared during fall of the Chelyabinsk meteorite on February 15, 2013. On separate days of July 2014 and 2015, there were layers of elevated aerosol scattering at heights of 11–15 km. Using back trajectory analysis, it was found that in these cases there was aerosol transport from the regions of pyrocumulus formation during forest fires in Canada.

Parameters of aerosol structures in the tropopause region and their relationship with the tropopause inversion layer are analyzed. The elevated aerosol content in the tropopause region as compared to its content in the known Junge layer, estimated according to the backscattering ratio, is observed in 33% of measurements (20% of crystalline-type structures and 13% of spherical-type structures). The probability of observation of a spherical-type aerosol layer increases by a factor of 1.4 in the presence of the tropopause inversion layer.

The data of these measurements were used to estimate the relative contributions of the lower (from tropopause to 15 km) and middle (15–30 km) stratospheric layers to the integrated optical characteristics of extinction and backscattering at a wavelength of 532 nm. It was found that the contribution of the lower layer to these extinction and backscattering characteristics exceeds the contribution of a middle layers by factors of 1.6 and 1.8, respectively. The total optical depth of the stratospheric aerosol, measured from the tropopause to 30 km, for background conditions is estimated at 0.012 with about a 60% relative contribution of the lower layer.

REFERENCES

1. O. Bazhenov, V. Burlakov, S. Dolgii, A. Nevzorov, and N. Salnikova, "Optical monitoring of characteristics of the stratospheric aerosol layer and total ozone content at the Siberian Lidar Station (Tomsk: 56°30′ N; 85° E)," Int. J. Remote Sens. **36** (11), 3024–3032 (2015). doi 10.1080/01431161.2015.1054964
2. T. Trickl, H. Giehl, H. Jager, and H. Vogelmann, "35 yr of stratospheric aerosol measurements at Garmisch-Partenkirchen: From Fuego to Eyjafjallajokull, and beyond," Atmos. Chem. Phys. **13** (10), 5205–5225 (2013).
3. S. S. Khmelevtsov, Yu. G. Kaufman, V. A. Korshunov, E. D. Svetogorov, and A. S. Khmelevtsov, "Laser sounding of atmospheric parameters at Obninsk Lidar Station SIU TYPHOON," in *Problems of Atmospheric Physics* (Gidrometeoizdat, St. Petersburg, 1998), p. 358–392 [in Russian].
4. V.A. Korshunov, D.S. Zubachev, E.G. Merzlyakov, and Ch. Jacobi, "Aerosol parameters of middle atmosphere by two-wavelength lidar sensing and their comparison with radio meteor echo measurements," Atmos. Ocean. Opt. **28** (1), 82–88 (2015).
5. V. A. Korshunov and D. S. Zubachev, "Determination of stratospheric aerosol parameters from two-wavelength lidar sensing data," Izv., Atmos. Ocean. Phys. **49** (2), 176–186 (2013).
6. S. Voigt, J. Orphal, K. Bogumil, and J. P. Burrows, "The temperature dependence (203–293) K of the absorption cross sections of O_3 in the 230–850 nm region measured by Fourier-transform spectroscopy," J. Photochem. Photobiol., A, Chem. **143** (1), 1–9 (2001).
7. L. T. Molina and M. J. Molina, "Absolute absorption cross sections of ozone in the 185- to 350-nm wavelength range," J. Geophys. Res., D **91** (13), 14501–14508 (1986).
8. J. P. Burrows, A. Richter, A. Dehn, B. Deters, S. Himmelmann, S. Voigt, and J. Orphal, "Atmospheric remote-sensing reference data from GOME: Part 2. Temperature-dependent absorption cross-sections of O_3 in the 231–794 nm range," J. Quant. Spectrosc. Radiat. Transfer **61** (4), 509–517 (1999).
9. Databases O3Spectra. http://www.iup.uni-bremen.de/gruppen/molspec/databases/referencespectra/o3spectra/index.html.
10. V. V. Zuev, *Lidar Control of the Stratosphere* (Nauka, Novosibirsk, 2004) [in Russian].
11. V. N. Ivanov, D. S. Zubachev, V. A. Korshunov, V. B. Lapshin, M. S. Ivanov, K. A. Galkin, P. A. Gubko, D. L. Antonov, G. F. Tulinov, A. A. Cheremisin, P. V. Novikov, S. V. Nikolashkin, S. V. Titov, and V. N. Marichev, "Lidar observations of stratospheric aerosol traces of Chelyabinsk meteorite," Opt. Atmos. Okeana **27** (2), 117–122 (2014).
12. T. Birner, A. Dornbrack, and U. Schumann, "How sharp is the tropopause at midlatitudes?," Geophys. Rev. Lett. **29** (14), 1700 (2002). doi 10.1029/2002GL015142
13. T. Birne, D. Sankey, and T. G. Shepherd, "The tropopause inversion layer in models and analyses," Geophys. Rev. Lett. **33**, L14804 (2006). doi 10.1029/2006GL026549
14. T. Deshler, R. Anderson-Sprecher, H. Jager, J. Barnes, D. J. Hofmann, B. Clemesha, D. Simonich, M. Osborn, R. G. Grainger, and S. Godin-Beekmann, "Trends in the nonvolcanic component of stratospheric aerosol over the period 1971–2004," J. Geophys. Res. **111**, D01201 (2006). doi 10.1029/2005JD006089
15. O. E. Bazhenov, V. D. Burlakov, S. I. Dolgii, and A. V. Nevzorov, "Lidar observations of aerosol disturbances of the stratosphere over Tomsk (56.5°N; 85.0°E) in volcanic activity period 2006–2011," Int. J. Opt. **2012**, Art. ID 786295 (2012). doi 10.1155/2012/786295
16. NASA. Global Sulfur Dioxide Monitoring. http://so2.gsfc.nasa.gov/measures.html.
17. Smithsonian Institution. Global volcanism program. http://volcano.si.edu.
18. M. From, O. Torres, D. Diner, D. Lindsey, B. Vant Hull, R. Servranckx, E. P. Shettle, and Z. Li, "Stratospheric impact of the chisholm pyrocumulonimbus eruption: 1. Earth-viewing satellite perspective," J. Geophys. Res. **113**, D08202 (2008).
19. M. Fromm, E. Shettle, K. H. Fricke, C. Ritter, T. Trickl, H. Giehl, M. Gerding, J. E. Barnes, M. O'Neill, S. T. Massie, U. Blum, I. S. McDermid, T. Leblanc, and T. Deshler, "Stratospheric impact of the Chisholm pyrocumulonimbus eruption: 2. Vertical profile perspective," J. Geophys. Res. **113**, D08203 (2008). doi 10.1029/2007JD009153
20. D. A. Ridley, S. Solomon, J. E. Barnes, V. D. Burlakov, T. Deshler, S. I. Dolgii, A. B. Herber, T. Nagai, R. R. Neely, III, A. V. Nevzorov, C. Ritter, T. Sakai, B. D. Santer, M. Sato, A. Schmidt, O. Uchino, and J. P. Vernier, "Total volcanic stratospheric aerosol optical depths and implications for global climate change," Geophys. Rev. Lett. **41** (22), 7763–7769 (2014). doi 10.1002/2014GL061541
21. L. Goldfarb, P. Keckhut, M.-L. Chanin, and A. Hauchecorne, "Cirrus climatological results from lidar measurements at OHP (44° N, 6° E)," Geophys. Rev. Lett. **28** (9), 1687–1690 (2001).
22. F. Immler and O. Schrems, "LIDAR Measurements of cirrus clouds in the northern and southern midlatitudes during INCA (55°N, 53°S): A comparative study," Geophys. Rev. Lett. **29** (16), 1809 (2002). doi 10.1029/2002GL015077
23. K. Sassen and J. R. Campbell, "A midlatitude cirrus cloud climatology from the facility for atmospheric remote sensing. Part I: Macrophysical and synoptic properties," Atm. Sci. **58** (5), 481–496 (2001).
24. O. A. Volkovitskii, L. N. Pavlova, and A. G. Petrushin, *Optical Properties of Crystal Clouds* (Gidrometeoizdat, Leningrad, 1984) [in Russian].
25. H. Jager and T. Deshler, "Correction to "Lidar backscatter to extinction, mass and area conversions for stratospheric aerosols based on midlatitude balloonborne size distribution measurements"," Geophys. Res. Lett. **30** (7), 1382 (2003). doi 10.1029/2003GL017189
26. Air Resources Laboratory. Transport & Dispersion Modeling, HYSPLIT. http://ready.arl.noaa.gov/HYSPLIT_traj.php.
27. CIMSS. PyroCb. http://pyrocb.ssec.wisc.edu/archives/370.
28. CIMSS. PyroCb. http://pyrocb.ssec.wisc.edu/archives/992#respond.

Translated by O. Bazhenov